JOURNAL OF GEOPHYSICAL RESEARCH, VOL. 112, A05216, doi:10.1029/2006JA011819, 2007

Magnetospheric Convection near a Drainage Plume

Chin S. Lin,[1] Huey-Ching Yeh,[2] Bill R. Sandel,[3] J. Goldstein,[4] Frederick J. Rich,[1] William J. Burke,[1] and J. C. Foster[5]

Received 27 April 2006; revised 3 December 2006; accepted 26 January 2007; published 24 May 2007.

[1] We report on equatorial convection associated with a plasmaspheric drainage plume using simultaneous observations from five satellites. During the early recovery phase of the July 2000 Bastille Day magnetic storm, the Extreme Ultraviolet sensor on the Magnetopause-to-Aurora Global Exploration satellite detected the plume near 16:00–17:00 magnetic local time extending outward to $L \approx 2.8$. The plasmaspheric boundary was near $L = 2$ at other local times. We mapped simultaneously measured ionospheric plasma drifts from ROCSAT-1 and three Defense Meteorological Satellite Program (DMSP) spacecraft along magnetic field lines to infer equatorial convection velocities in the inner magnetosphere. The zonal component of convection derived from ROCSAT-1 ion-drift measurements had a sharp, positive azimuthal gradient near the plume's boundaries, reversing direction from westward to eastward. The meridional profile of horizontal velocities deduced from DMSP measurements shows a large, westward-flowing subauroral polarization stream (SAPS) located outside the plasmapause. The peak velocity of the SAPS centered at a radial distance of $L \approx 2.8$ with a full width of $\sim 1\ R_E$. In the inertial frame of reference, equatorial plasmas flowed toward the plume from both its day and evening sides, suggesting a negative gradient in the equatorial azimuthal velocity that was largest near the plume's outermost boundary. These observations provide new evidence about diversion of SAPS plasma flows and distinctive azimuthal velocity patterns in the vicinity of plasmaspheric plumes.

Citation: Lin, C. S., H.-C. Yeh, B. R. Sandel, J. Goldstein, F. J. Rich, W. J. Burke, and J. C. Foster (2007), Magnetospheric Convection near a Drainage Plume, *J. Geophys. Res.*, *112*, A05216, doi:10.1029/2006JA011819.

1. Introduction

[2] Drainage plumes are by-products of the plasmapause's inward motion during geomagnetic disturbances, a process known as plasmasphere erosion. Their dynamics have been described as superposed effects of convection, shielding, and corotation [*Grebowsky*, 1970; *Chen and Wolf*, 1972; *Spiro et al.*, 1981; *Weiss et al.*, 1997; *Lambour et al.*, 1997; *Goldstein et al.*, 2004]. Cold plasma flow follows equipotential lines. In the dusk sector, the superposed dawn-to-dusk and the corotational electric fields cause equipotential lines to map radially outward, defining the bulged plasmaspheric boundary [*Chen and Wolf*, 1972]. The build-up of pressure in the asymmetric ring current during the late main phase of large geomagnetic storms significantly distorts the local magnetic field, contributing to a premidnight plasmapause bulge. The asymmetric ring current also couples to the ionosphere via field-aligned currents concentrating westward-flowing plasma into subauroral polarization streams (SAPS) that contribute to drainage plumes in the equatorial plane [*Goldstein et al.*, 2003a; *Mishin et al.*, 2003; *Goldstein et al.*, 2004].

[3] Plasma flow velocities in the outer plasmasphere have been measured by the Magnetospheric Plasma Analyzer (MPA) instrument onboard the Los Alamos National Laboratory (LANL) geosynchronous satellites [*Ober et al.*, 1997; *Borovsky et al.*, 1998; *Thomsen et al.*, 1998; *Goldstein et al.*, 2004]. These studies showed that the average flow velocity inside enhanced cold density structures is generally a few kilometers per second sunward in the inertial frame at geosynchronous orbit. In particular, *Goldstein et al.* [2004] reported in situ measurements of sunward plasma flow by the LANL satellite passing through a drainage plume in the late afternoon sector observed simultaneously by the Extreme Ultraviolet (EUV) sensor on the Imager for Magnetopause-to-Aurora Global Exploration (IMAGE) satellite. They pointed out that the flow-speed data fluctuated quite a bit, probably related to an uncertainty in the flow-speed measurements made by the MPA. Although the accuracy of the MPA measurements is difficult to estimate, the data indicate that average flow speeds increase on the eastward side of the plume and are probably related to ongoing SAPS events. So far, no direct plasma measurements have been reported

[1] Air Force Research Laboratory, Space Vehicles Directorate, Hanscom AFB, Bedford, Massachusetts, USA.
[2] Institute of Space Science, National Central University, Jhongli, Taiwan.
[3] Lunar and Planetary Laboratory, University of Arizona, Tucson, Arizona, USA.
[4] Southwest Research Institute, San Antonio, Texas, USA.
[5] Haystack Observatory, MIT, Westford, Massachusetts, USA.

0148-0227/07/2006JA011819$09.00

that specify the radial distributions of equatorial plasma motion in and near plumes. Multisatellite observations reported here help fill this gap.

[4] The overlap of a SAPS convection event with the outer portion of a drainage plume was reported by *Foster et al.* [2002]. They found that storm-enhanced density (SED) channels of elevated total electron content in the ionosphere are associated with the erosion of the outer plasmasphere. *Foster et al.* [2004] projected the Global Positioning System observations of the SED from the 350-km ionospheric penetration altitude into the magnetospheric equatorial plane using the T01 magnetic field model in the Geocentric Solar Magnetospheric (GSM) coordinate system [*Tsyganenko*, 2002]. They used this mapping to show that the erosion flux in the high-altitude region is related to flow from the plasmasphere toward the dayside magnetopause. In this paper, we have adopted the T01 magnetic field model to map plasma convection in the evening sector between the ionosphere and the equatorial plane.

[5] The EUV sensor on the IMAGE satellite provided global views of inner magnetospheric dynamics by imaging the distribution of resonantly scattered 30.4-nm solar radiation from He^+ ions in the plasmasphere [*Sandel et al.*, 2001]. The EUV images show plumes as narrow regions of enhanced He^+ density that connect to the main plasmasphere, usually in the late afternoon sector. Typical plumes range in size from 3 to 5 R_E in length and from 0.5 to 1 R_E in width [*Sandel et al.*, 2003]. The EUV instrument observed persistent plume features from 01:00 to 06:00 Universal time (UT) on 16 July 2000, during the early recovery phase of the Bastille Day magnetic storm. Available images indicate that the plasmasphere was confined close to Earth ($L \leq 2$). An example is shown in Figure 1a.

[6] Identifying plasmaspheric boundaries in EUV images depends on the detector's sensitivity. The effective lower EUV detection threshold has been characterized during quiet or mildly disturbed intervals and is equivalent to $\sim 40 \pm 10$ electrons/cm^{-3} [*Goldstein et al.*, 2003b; *Moldwin et al.*, 2003]. This EUV density threshold is found to be consistent with the densities measured by Cluster during a plasmasphere crossing in conjunction with IMAGE EUV observations [*Darrouzet et al.*, 2004]. For a plasmasphere with 10% He^+, this EUV detection threshold corresponds to a density of 3–5 He^+ cm^{-3}. If the He^+/H^+ ratio is nonuniform, the He^+ density boundary would differ from the hydrogen plasmaspheric boundary. The plasmasphere density boundary observed at lower L shells during severe magnetic disturbances should be relatively sharp if the plasmasphere depletes quickly. An informal survey of upper hybrid resonance frequencies measured by the Combined Release and Radiation Effects Satellite indicates that near $L = 2$ electron densities ranged from 400 to >1600 cm^{-3} both in quiet times and during the three major magnetic storms of 1991. We note that the noise in EUV images was much higher than normal during this time. Thus, we suspect that during the Bastille Day storm, the EUV detection threshold for He^+ was significantly higher than the 3–5 He^+ cm^{-3}.

[7] While IMAGE was observing the drainage plume, the ROCSAT-1 satellite was flying in the low-latitude ($1.1 < L < 1.8$) ionosphere where it detected unusual ion-convection signatures. Three polar-orbiting spacecraft of the Defense Meteorological Satellite Program (DMSP F12, F13, and F15) simultaneously measured the cross-track (mostly east-west) component of ionospheric plasma drifts in the late-afternoon and early evening sectors. The DMSP satellites complement the observations with the radial profiles of convection related to the plasmaspheric plume in L shells between 1.5 and 4. They also provide information about the relative position of SAPS with respect to the plume and the plasmaspheric boundary.

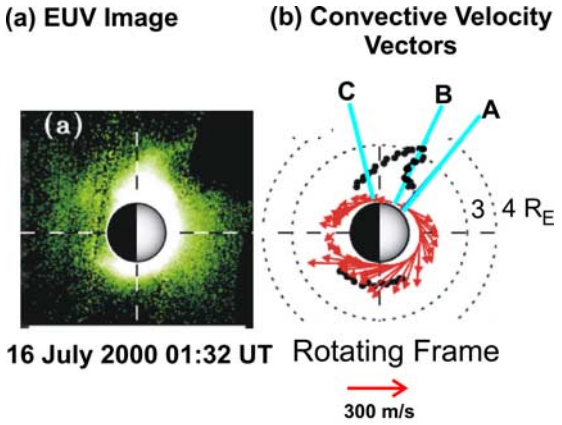

Figure 1. (a) EUV image of a plasmaspheric plume acquired by IMAGE at 01:32 UT and (b) ROCSAT-1 convective velocity vectors mapped to the equatorial plane during a complete orbit from 00:40 UT to 02:16 UT on 16 July 2000. The dark circles in Figure 1b mark the position of the He^+ plasmaspheric boundary determined from the EUV image. Line A corresponds to the location where the He^+ plasmaspheric boundary starts to bulge, line B marks the plume's dayside edge, and line C marks the nightside edge of the plume. The velocity vectors in Earth's corotating frame of reference are plotted as red vectors at every half hour in MLT. The dotted lines at radial distance 3 and 4 R_E are plotted for coordinate reference. A vector with a length equal to 300 m/s is shown as a scale for the velocity vectors.

[8] Section 2 of this paper briefly describes the procedures used to map ion drifts from the ionosphere to the equatorial plane. We then present simultaneous measurements from the ROCSAT-1, DMSP, and IMAGE satellites in section 3. Differences between zonal-drift patterns observed in the main and recovery phase are described briefly in section 4. Observational results are summarized and their implications discussed in section 5; conclusion is in section 6.

2. Data Sources and Methodology

[9] ROCSAT-1 was launched on 27 January 1999 into a 600-km circular orbit at an inclination of 35°. The Ionospheric Plasma and Electrodynamics Instrument payload contained an ion trap, two drift meters, and a retarding potential analyzer [*Yeh et al.*, 1999] from which we deduce the two components of the convection velocity V_Z and V_M. V_Z, the zonal component, is positive toward the east; V_M, the radial component, is positive in the outward direction [*Lin and Yeh*, 2005]. From these velocity components, we calculate two components of convective electric fields E_M and E_Z at the satellite altitude, $\mathbf{E} = -\mathbf{V} \times \mathbf{B}$, where $\mathbf{V}$ and $\mathbf{B}$

are the convection and magnetic field vectors at the satellite location, respectively. We then use the relationships derived by *Mozer* [1970] to calculate equatorial electric fields from ionospheric values,

$$E_{\mathrm{Mi}} h_{\mathrm{i}} = E_{\mathrm{Me}} h_{\mathrm{e}} \tag{1}$$

and

$$E_{\mathrm{Zi}} d_{\mathrm{i}} = E_{\mathrm{Ze}} d_{\mathrm{e}} \tag{2}$$

Here h is the perpendicular distance between neighboring field lines in the meridional plane, and d is the distance perpendicular to the meridional plane between neighboring field lines. The subscripts i and e denote locations in the ionosphere and at the equator, respectively. The equatorial convective velocity $\mathbf{V}_{\mathrm{e}}$ is calculated from equatorial electric field $\mathbf{E}_{\mathrm{e}}$ and equatorial magnetic field $\mathbf{B}_{\mathrm{e}}$ by the definition $\mathbf{V}_{\mathrm{e}} = (\mathbf{E}_{\mathrm{e}} \times \mathbf{B}_{\mathrm{e}}) / \mathbf{B}_{\mathrm{e}}^2$. The ratio of zonal convection velocities between the equatorial plane and the ionosphere is then

$$\frac{V_{\mathrm{Ze}}}{V_{\mathrm{Zi}}} = \frac{E_{\mathrm{Me}} \mathbf{B}_{\mathrm{i}}}{E_{\mathrm{Mi}} \mathbf{B}_{\mathrm{e}}} = \frac{h_{\mathrm{i}} \mathbf{B}_{\mathrm{i}}}{h_{\mathrm{e}} \mathbf{B}_{\mathrm{e}}} \tag{3}$$

The ratio of meridional convection velocities in the equatorial plane and the ionosphere is

$$\frac{V_{\mathrm{Me}}}{V_{\mathrm{Mi}}} = \frac{E_{\mathrm{Ze}} \mathbf{B}_{\mathrm{i}}}{E_{\mathrm{Zi}} \mathbf{B}_{\mathrm{e}}} = \frac{d_{\mathrm{i}} \mathbf{B}_{\mathrm{i}}}{d_{\mathrm{e}} \mathbf{B}_{\mathrm{e}}} \tag{4}$$

For a dipole magnetic field model, *Mozer* [1970] showed that

$$\frac{V_{\mathrm{Ze}}}{V_{\mathrm{Zi}}} = L^{3/2} \tag{5}$$

and

$$\frac{V_{\mathrm{Me}}}{V_{\mathrm{Mi}}} = L(4L - 3)^{1/2} \tag{6}$$

where L represents the distance from the center of the dipole to the intersection of a field line with the magnetic equatorial plane. To estimate equatorial convective velocities from the ROCSAT-1 data, we must determine approximately the L value and the ratios of $h_{\mathrm{e}}/h_{\mathrm{i}}$, $d_{\mathrm{e}}/d_{\mathrm{i}}$, and $\mathbf{B}_{\mathrm{e}}/\mathbf{B}_{\mathrm{i}}$ by tracing magnetic field lines from ROCSAT-1's position in the ionosphere to the equatorial plane. The International Geomagnetic Reference Field (IGRF) magnetic field model was used in the calculation.

[10] DMSP satellites measure the cross-track, horizontal component of plasma velocity in the ionosphere. Because the DMSP measurements of interest were acquired outside the plasmasphere, the IGRF magnetic field model may not adequately account for the magnetic field inflation. Thus, when mapping the horizontal component of DMSP plasma velocity, we used the Tsyganenko T01 magnetic field model [*Tsyganenko*, 2002] to trace magnetic field lines from DMSP locations in the ionosphere to the equatorial plane. To distinguish from the equatorial zonal velocities deduced from ROCSAT-1 data, we refer to the equatorial horizontal velocity determined from the DMSP data as the equatorial azimuthal velocity. We normally calculate DMSP measurements of ion drift velocity in Earth's corotating frame by subtracting the corotational velocity at the topside ionosphere. Here we express equatorial azimuthal velocities in the inertial frame by adding the corotational velocity in the equatorial plane to the equatorial horizontal velocity in Earth's corotating frame.

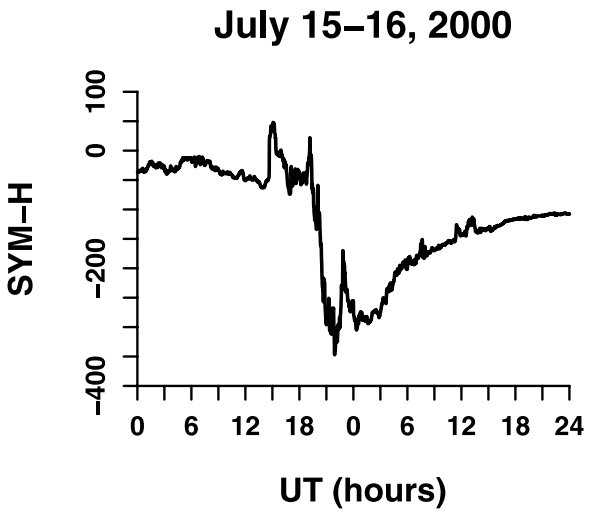

Figure 2. Time history of the Sym-H index for 15–16 July 2000.

3. Observations

[11] The Bastille Day storm started at 19:50 UT on 15 July 2000 when magnetic activity was already very intense (Kp = 9). Figure 2 illustrates the storm's evolution in terms of the time history of the Sym-H index. The peak intensity of the storm occurred at ~22:00 UT on 15 July 2000, and recovery began early on 16 July. Because of intense solar-proton fluxes, IMAGE failed to acquire clear EUV images before 16 July that might elucidate the plume's main-phase evolution. However, the EUV imager did observe a plasmaspheric drainage plume for 4 hours starting at ~00:50 UT on 16 July. Figure 1a shows the EUV image acquired at 01:32 UT. During this severe magnetic storm, the EUV images show the dayside boundary close to 2 R_{E} with a plume protruding to ~2.8 R_{E} near 16:20 magnetic local time (MLT). In the evening sector, the He^+ plasmaspheric boundary reverted to ~2 R_{E}.

[12] The He^+ density boundary estimated from the EUV image taken near 01:32 UT is represented by solid circles in Figure 1b. Figure 1b contains three lines, A at ~15:00 MLT roughly corresponds to the place where the plasmaspheric bulge started, B at ~16:00 MLT extends along the plume's dayside edge, and C at ~ 19:00 MLT marks the plume's nightside edge. To investigate correlations between ROCSAT-1 observations and the plasmaspheric plume, we present ion velocity measurements for a complete orbit of ROCSAT-1 from 00:40 to 02:16 UT. Close in time to the 01:32 UT EUV image, ROCSAT-1 made plasma drift measurements near 16:20 MLT. For this orbit, the L values sampled by ROCSAT-1 varied from 1.1 to 1.6. Figure 1b indicates that the equatorial

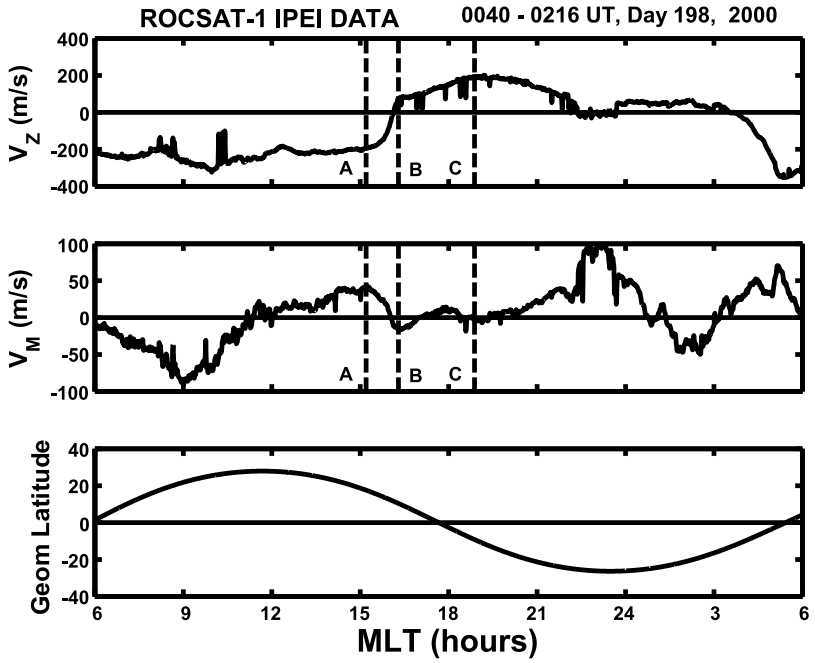

Figure 3. Components of equatorial convective velocity deduced from ROCSAT-1 data as functions of MLT. The top panel shows the zonal component V_Z, and the second panel plots the radial component V_M. The geomagnetic latitude of ROCSAT-1 is plotted in the bottom panel. Vertical lines A, B, and C correspond to three radial lines shown in Figure 1b.

convection after removal of corotation was generally westward before 16:00 MLT and eastward after 16:00 MLT. Thus, ROCSAT-1 data indicate a reversal of equatorial convection velocity in the corotating frame of reference at the plume longitude determined from the EUV image.

3.1. Rocsat-1 Observations

[13] The zonal and radial components of plasma velocity mapped to the equatorial plane in the Earth's corotating frame are plotted as functions of MLT in the top two panels of Figure 3 for the same interval as Figure 1b. The bottom panel presents the magnetic latitude of ROCSAT-1. The zonal velocity V_Z (top panel of Figure 3) was nearly constant at about -250 m/s on the dayside and increased sharply near 15:00 MLT (line A), roughly matching the MLT of the sunward boundary of the plume detected by IMAGE (line A in Figure 1b). The zonal velocity reversed direction near the plume MLT denoted by line B. The MLT of the plume's nightside boundary in the EUV image corresponds to the peak eastward zonal velocity, $\sim$200 m/s (line C in Figure 3). The radial component of velocity V_M was generally small (<50 m/s) and outward between 12:00 and 21:00 MLT (middle panel, Figure 3).

[14] Figure 4 displays the equatorial zonal velocity U_Z in Earth's inertial frame of reference (top panel) and its corresponding L values (bottom panel). Since the radial velocity in the inertial frame is the same as in the corotating frame (Figure 3), it is not repeated here. The horizontal dashed curve represents the corotation velocity in the equatorial plane at the radial distance of L. Figure 4 indicates that U_Z along ROCSAT-1's orbital trajectory was roughly constant and subcorotational in the dayside from 05:00 to 15:00 MLT. Similar to V_Z, U_Z had a sharp positive azimuthal gradient of $\sim$600 m s^{-1} MLT^{-1} between 15:30 and 16:00 MLT. From 16:00 to 03:00 MLT on 16 July, equatorial plasma appeared to drift at supracorotational

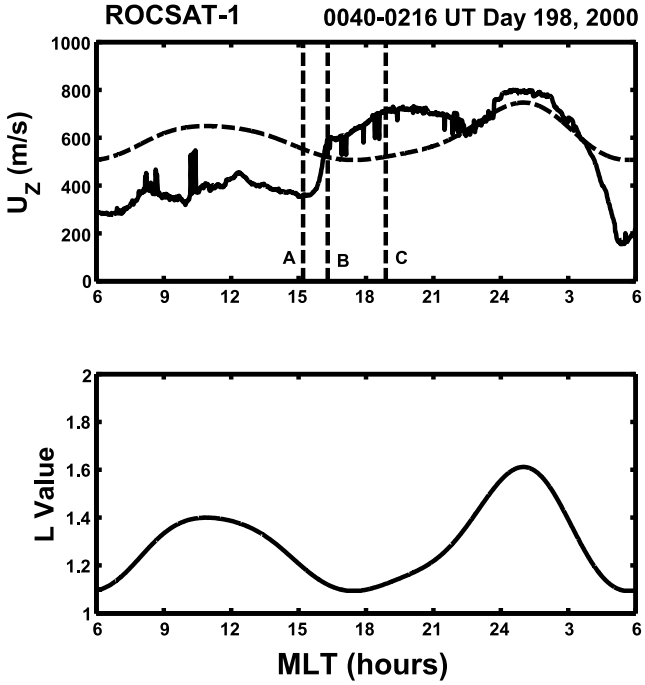

Figure 4. Equatorial zonal velocity component in Earth's inertial frame (top panel) and L value (bottom panel) as a function of MLT for the ROCSAT-1 orbit shown in Figure 3. The dashed curve is the corotation velocity in the equatorial plane for the given L. Vertical dashed lines A, B, and C are defined as in Figure 1b.

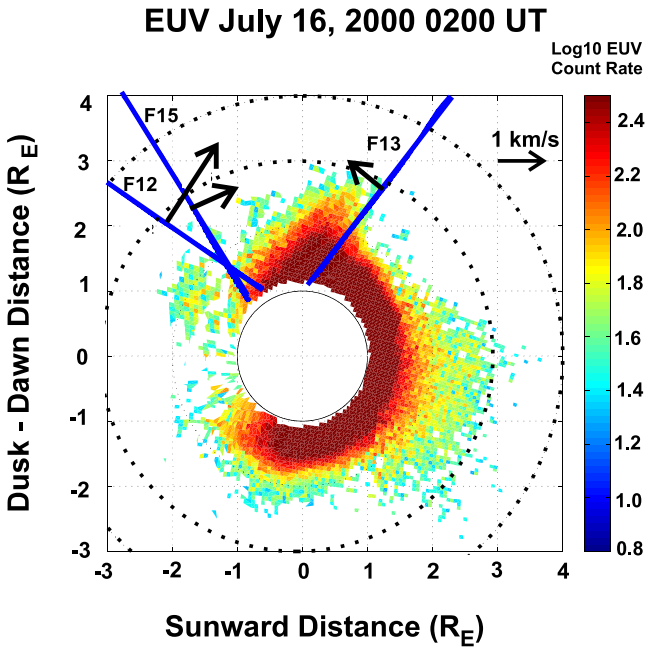

Figure 5. EUV image of the He^+ plasmasphere mapped to the equatorial plane in GSM coordinates. Trajectories of three DMSP satellites mapped to the equatorial plane are overlaid on the EUV image. Arrows on the DMSP satellite tracks indicate the directions of convection. A scale of the velocity vector is shown in the upper right corner.

speeds with minor variations. Thus, equatorial plasma zonal flow was subcorotational before the plume's MLT (line A) and became supracorotational after it (line B).

3.2. DMSP Observations

[15] During the interval 01:45–02:10 UT, DMSP satellites measured ionospheric drifts at longitudes near the MLT sector of the He^+ plasmaspheric plume. Figure 5 shows the EUV snapshot of the He^+ plasmasphere acquired at 02:02 UT and mapped to the equatorial plane in GSM coordinates. For each pixel of the EUV image, the X, Y, and Z coordinates of points of minimum L along observing lines of sight from IMAGE were first computed, assuming a dipole field. These points were then mapped to the GSM equatorial plane ($Z = 0$) using the magnetic field model of *Tsyganenko* [2002] calculated for the times of observations. Figure 5 indicates that the He^+ plume's outer boundary remained at $\sim$2.8 R_E. Similarly, the orbital tracks of three DMSP satellites (F12, F13, and F15) in the topside ionosphere near the time of this EUV image were projected to the GSM $Z = 0$ plane in order to give the best multi-instrument comparison of the observed features. Projected MLTs for DMSP satellites in the equatorial plane are about an hour lower than their locations in the ionosphere. The projected F13 locus on the GSM equatorial plane passed through the plume's dayside edge along a trajectory from 17 MLT to 16.1 MLT as it moved from $L = 1.5$ (01:50 UT) to $L = 4$ (01:58 UT). The mapped F12 and F15 loci followed similar trajectories passing outside the plume in the 20:00–21:00 MLT range. The F15 locus moved from the 20:48 MLT meridian at $L = 1.5$ (02:00 UT) to the 20:20 MLT at $L = 4$ (02:07 UT). F12's projected trajectory was slightly further to the nightside, moving from the 21:12 MLT meridian at $L = 4$ (01:59 UT) to the 20:24 MLT meridian at $L = 1.5$ (02:06 UT). We placed arrows along the mapped DMSP trajectories in Figure 5 to indicate azimuthal velocities at $\sim$2.8 R_E. F13 measured an eastward azimuthal velocity of $\sim$1 km/s at the dayside edge of the plume; F12 and F15 detected westward azimuthal velocities in the evening sector of about −2 and −1 km/s, respectively.

[16] Figure 6 shows the radial profiles of equatorial azimuthal velocities deduced from mapping DMSP horizontal velocities to the equator for the time interval corresponding to Figure 5. During this time period, DMSP F12 measured flow in the Southern Hemisphere, whereas F13 and F15 measured flow in the Northern Hemisphere. Assigned L values were determined by tracing the field line from DMSP to the GSM equatorial plane. In the Tsyganenko model, magnetic field lines tend to stretch tailward during severe magnetic disturbance. Thus, the assigned L value is larger than that of a dipole field by an amount proportional to geomagnetic latitude. For instance, in the storm's early recovery, the field line of $L = 3$ in a dipolar magnetic field is mapped from DMSP's altitude to $\sim$4 R_E in the T01 model. The legend in Figure 6 shows the MLT of the projected DMSP loci on the equatorial plane at 3 R_E radial distance. The projected MLT was 16.3 for F13, 20.4 for F15, and 21.1 for F12. The figure also represents the

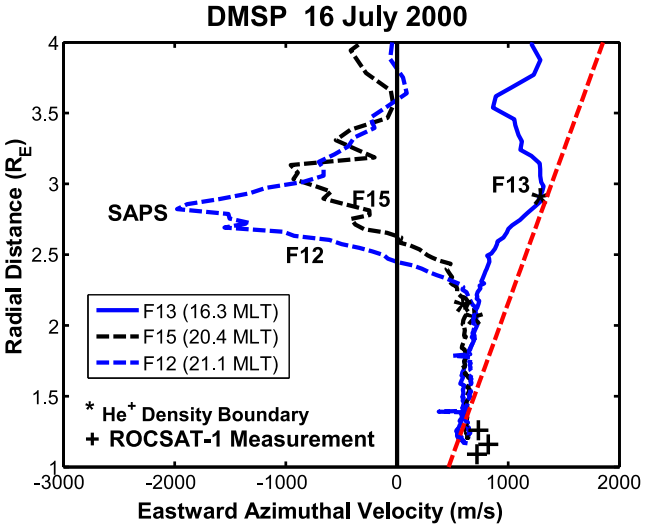

Figure 6. Radial profiles of the equatorial azimuthal velocity deduced from DMSP ion drift data near 02:00 UT on day 198, 16 July 2000, with F13 at 16.3 MLT (blue solid line), F15 at 20.4 MLT (black dashed line), and F12 at 21.1 MLT (blue dashed line). The straight red dashed line represents the corotational velocity. The azimuthal velocity is positive in direction of the corotation (eastward). Large westward azimuthal flows are associated with SAPS. Locations of the He^+ plasmaspheric boundary are represented by an asterisk on the velocity profiles for each satellite. ROCSAT-1 velocities at the MLT of the three DMSP satellites are represented with plus signs at L values around 1.2.

plasma corotation velocity as a red straight dashed line. For consistency with the ROCSAT-1 data presentation, we define DMSP eastward azimuthal velocities in the direction of the corotation to be positive. Note that this definition of equatorial azimuthal velocity differs from the common presentation of horizontal velocity measured by DMSP. At the dayside edge of the plume, F13 observed an eastward azimuthal velocity slightly less than the corotation velocity for $L < 2.8$ near the outermost boundary of detectable 30.4-nm photons as marked by an asterisk. Outside this He^+ density boundary, the azimuthal component of plasma velocity decreased almost linearly with radial distance. At $L = 4$, the equatorial eastward azimuthal velocity was ~30% less than the corotation velocity.

[17] At radial distance $L < 2.1$, both F12 and F15 detected about the same equatorial eastward azimuthal velocities as F13. For this event, DMSP satellites measured eastward azimuthal velocities lower than Earth's corotational velocity for $L > 1.3$ and slightly faster than Earth's corotational velocity for $L < 1.3$. Figure 4 indicates that the equatorial zonal velocity measured by ROCSAT-1 at $L < 1.3$ was also faster than the Earth's corotational velocity between 18 and 21 MLT. The DMSP velocity measurements agreed with ROCSAT-1 measurements in direction because both satellites measured suprarotational velocities. We compare ROCSAT-1 equatorial zonal velocity at locations close to the three DMSP satellites with the DMSP measurements in Figure 6. ROCSAT-1 velocities at the MLT of the three DMSP satellites are presented with "+" symbols at L values around 1.2. The DMSP velocity measurements appeared to be smaller than ROCSAT-1 measurements by about 100 m/s. The difference in measurements is within the variation of instrument calibration limits between the two satellites.

[18] The EUV image placed the He^+ plasmaspheric boundary near $L = 2.1$ in the 20:00–21:00 MLT sector where F12 and F15 crossed it (marked by an asterisk). Beyond the He^+ boundary ($L > 2.1$), the azimuthal velocity in the 20:00–21:00 MLT sector deviated substantially from the corotation velocity. Between $L = 2.5$ and 3.5, the azimuthal velocity was negative, indicating strong westward flows that reached ~2 km/s near the outermost boundary of the plume ($L = 2.7$). Azimuthal velocity profiles observed by F12 and F15 in the evening hours replicate SAPS signatures described by *Foster and Vo* [2002]. The DMSP and IMAGE observations during this event suggest that in the evening sector, plasma flow had a strong, westward component outside the He^+ density boundary. However, this signature of westward SAPS flow was absent in the F13 radial profile. The comparison of F15 and F13 velocity profiles indicates that the westward component of the SAPS velocity inside $L = 3.5$ diminished between 20.4 and 16.3 MLT, before reaching the F13 MLT. By comparing the F12 and F15 velocity profiles, we estimate that at $L = 2.8$, the SAPS azimuthal velocity decreased by a factor of 4 between 21:00 and 20:00 MLT. The SAPS azimuthal velocity reduction appeared to be confined to $L < 3$.

[19] Another outstanding feature of the DMSP data is that the equatorial plasmas convected toward the plume in the inertial frame. Recall that from $L = 2.5$ to 3.5 plasma eastward azimuthal velocities were positive before the plume's MLT and negative thereafter. This implies a negative azimuthal gradient in azimuthal velocity across the plume from 16.5 to 20 MLT. The large azimuthal gradient was mainly confined to the radial range of the SAPS with the largest gradient located at the outermost boundary of the plume. We emphasize that outside the He^+ density boundary ($L > 2$), the direction of the azimuthal velocity gradient was opposite to that observed by ROCSAT-1 at $L < 1.5$.

4. Temporal Variations of Zonal Velocity

[20] Figure 7 compares ROCSAT-1 ion-drift observations in the afternoon and evening sectors (12:00–21:00 MLT) with solid and dashed lines representing plasma velocities measured during the main phases and the early recovery phases, respectively. In this MLT sector, ROCSAT 1 measured main-phase ion velocities between 23:26 UT (day 197) to 00:04 UT (day 198) and early recovery drifts on the subsequent orbit between 01:03 and 01:41 UT (day 198). Because velocity measurements acquired after 21:00 MLT are not relevant to the present work, they are not displayed. The geomagnetic latitude varied from 30° at 12 hours MLT to −20° at 21 hours MLT (bottom panel). During the main phase, the zonal velocity V_Z remained less than 50 m/s from 12:00 to 15:00 MLT and then increased to ~200 m/s after 16:00 MLT (solid black line, top panel). The distinctive difference between the two orbits is an extension of large westward flow ($V_Z \sim -200$ m/s) from 12:00 to 16:00 MLT during recovery (red dashed line, top panel). Figure 7 thus indicates that the sharp reversal of the zonal velocity in the afternoon sector was a recovery-phase feature that did not appear during the main phase. In the afternoon and evening sectors, V_M manifested no distinctive characteristics either during the main or recovery phases (middle panel).

[21] Figure 8 provides more information about the temporal variation of V_Z between 16:00 UT (day 197) and 06:00 UT (day 198). Before storm onset (19:00 UT, day 197), the hourly averaged value of V_Z at 15:00 MLT (solid dots in Figure 8) was larger than at 21:00 MLT (triangles), indicating a negative azimuthal gradient (shown as downward pointing arrows). Immediately after onset, ROCSAT-1 detected large ($V_Z < -400$ m/s) westward surges at both 15:00 and 21:00 MLT. However, in the next two main-phase orbits, ROCSAT-1 detected V_Z that was positive at 15:00 and negative at 21:00 MLT, again indicating a negative azimuthal-velocity gradient. After the storm recovery (> 01:00 UT, day 198), the zonal velocity reversed; V_Z switched from large and negative at 15:00 MLT to large and positive at 21:00 MLT. The azimuthal gradient in V_Z thus reversed to positive (upward pointing arrows). Finally, as recovery continued, the differences in V_Z between 15:00 and 21:00 MLT decreased to negligible amounts. Thus, the positive azimuthal gradient of the zonal velocity appears to have occurred in the late afternoon only during the recovery phase.

5. Discussion

[22] Simultaneous observations from IMAGE, ROCSAT-1, and DMSP satellites during the early recovery phase of the July 2000 magnetic storm yield complementary views of plasmaspheric convection in the vicinity of the plasmaspheric plume. ROCSAT-1 data indicate that in the late afternoon, sector zonal velocity V_Z changed from eastward

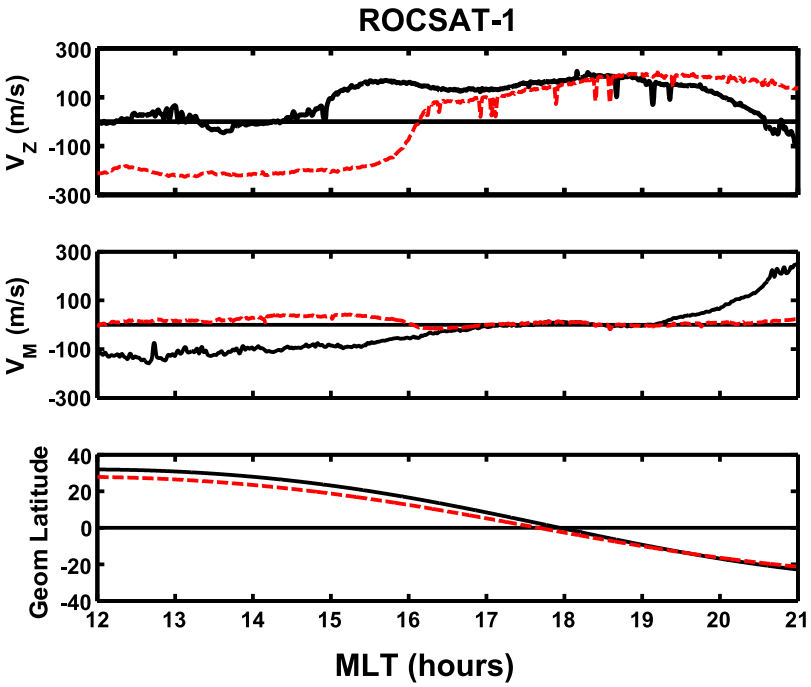

Figure 7. Comparison of plasma convection velocities measured by ROCSAT-1 in the 12–21 MLT range during two consecutive orbits on 15 and 16 July 2000. The figure format is the same as Figure 3. Measurements during the first orbit from 23:26 UT (day 197) to 00:04 UT (day 198) are marked in solid lines. Data acquired during the next orbit (01:03–01:41 UT, day 198) appear as red dashed lines. The first/second orbit occurred during the storm's main/early recovery phase.

during the main phase to westward during the recovery. In the evening sector, V_Z displayed an opposite behavior changing from westward during the main phase to eastward during the recovery. At low L shells surveyed by ROCSAT-1, the zonal velocity had a sharp positive gradient near the plume's longitude. However, the azimuthal velocity gradient observed by the DMSP satellites near the plume's outermost boundary is in the opposite direction. In the inertial frame, equatorial plasmas in the outer plasmasphere convect toward the plume from both of its sides, suggesting a large negative azimuthal velocity shear across the plume, mainly with radial distance in the range $2 \leq L \leq 3.5$, associated with observed SAPS structures. This feature was never pointed out before, perhaps because DMSP data are usually examined in Earth's corotating frame where azimuthal velocity shears are not obvious.

[23] *Basu et al.* [2001] and *Lin et al.* [2001] previously described ion drifts detected by ROCSAT-1 during the July 2000 magnetic storm. *Basu et al.* [2001] showed that ROCSAT-1 detected large ion drifts in the southward, westward, and upward directions in the 21:00–02:00 MLT sector at the beginning of the main phase. During three passes distributed throughout the main phase of this storm, ROCSAT-1 observed large south-westward flows near the SAA [*Lin et al.*, 2001]. These two previous reports on ROCSAT-1 observations did not note the zonal velocity reversal studied in this paper.

[24] *Heelis and Coley* [1992] used drift meter measurements from the polar-orbiting DE-2 satellite to study the statistical behavior of zonal plasma velocities in the low-latitude ionosphere. *Vickrey et al.* [1979] and *Fejer et al.* [1991] investigated the diurnal variations of zonal velocities using incoherent scattered radar data. They generally found weak zonal-velocity reversals near dusk but gave them no

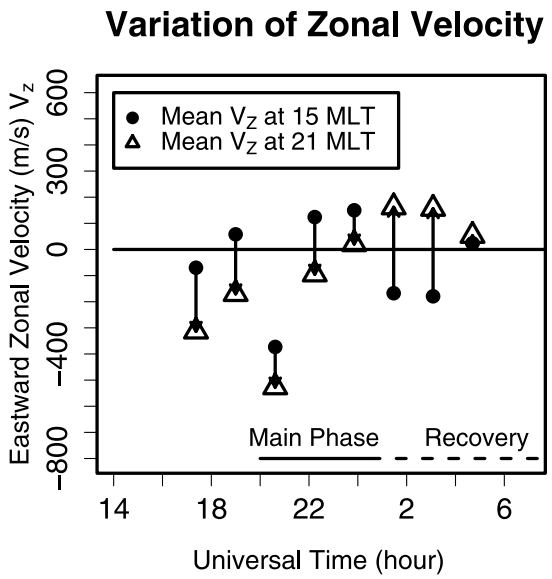

Figure 8. Temporal variation of two hourly averaged zonal velocities V_Z from 16:00 UT, day 197 to 06:00 UT, day 198. The hourly averaged V_Z at 15:00 and 21:00 MLT are shown as dots and triangles, respectively. The arrows on lines connecting V_Z values at 15:00 and 21:00 MLT represent the directions of zonal-velocity gradients (positive/negative gradients correspond to upward/downward arrows).

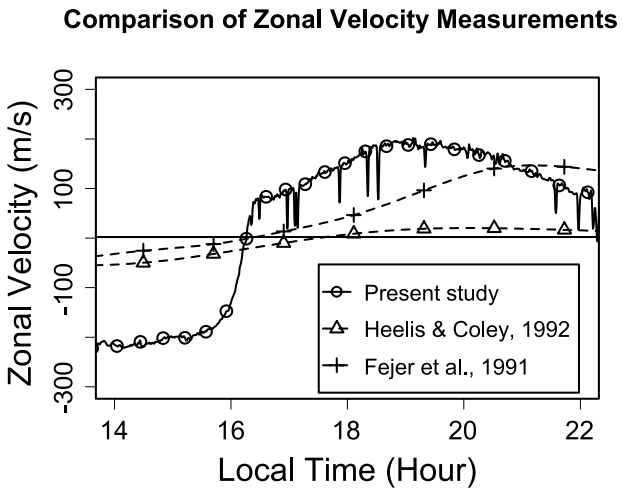

Figure 9. Comparison of zonal velocities measured by ROCSAT-1 from 14:00 to 22:00 MLT during the orbit shown in Figure 3 with statistically averaged zonal velocities reported by *Fejer et al.* [1991] and *Heelis and Coley* [1992].

great emphasis. Figure 9 compares the statistical averages deduced by *Heelis and Coley* [1992] and by *Fejer et al* [1991] with the zonal velocity reversal observed by ROCSAT-1 between 14:00 and 22:00 LT. *Heelis and Coley* [1992] analyzed the statistics of zonal ion drifts as functions of local time at various invariant latitudes between 25° and 65° during magnetically quiet and disturbed periods. At 25° latitude, DE 2 data showed that, on average, zonal ion drifts crossed from westward velocity to eastward velocity near dusk. The average azimuthal gradient of V_Z was positive at 18:00 MLT, increasing from −60 m/s at 15:00 MLT to 20 m/s at 20:00 MLT during disturbed times (diamond dashed line, Figure 9). The azimuthal velocity gradient observed by ROCSAT-1 during the July 2000 storm recovery was much sharper than the DE 2 average and confined to a half-hour band in local time (solid line, Figure 9). *Fejer et al.* [1991] calculated seasonal averages of zonal plasma drifts in the equatorial F layer of the ionosphere above Jicamarca, Peru. The average zonal drift in the evening sector was much larger than that reported by *Heelis and Coley* [1992] using DE-2 measurements. The average zonal drift increases from −60 m/s at 12:00 LT to ∼120 m/s at 20:00 LT with a gradual positive azimuthal gradient, almost independent of magnetic activity (plus sign dashed line, Figure 9). ROCSAT-1 observations of zonal velocity gradients near dusk differ from the seasonal averages reported by *Fejer et al.* [1991] not only in magnitude but also in the dependence on magnetic activity. The sharp zonal velocity reversal seen in the late afternoon on 16 July 2000 was clearly a storm recovery phenomenon as demonstrated in Figures 7 and 8.

[25] Observed zonal velocity reversals are signatures of stormtime electric fields in the inner magnetosphere and midlatitude to low-latitude ionosphere that represent superposed effects of multiple, interacting sources. The first source is penetration electric fields (PEFs), which we describe as electric fields of magnetospheric origin whose effects are most readily observed during magnetic storms in the subauroral ionosphere by satellites and/or ground based radar [*Burke*, 2006; *Huang et al.*, 2006]. PEFs in the magnetosphere are responsible for the energization and earthward movement of the ring current. Large-scale field aligned currents that couple the magnetosphere and ionosphere produce the distribution of potential needed to maintain force balance in the magnetosphere and current continuity in the ionosphere [*Vasyliunas*, 1970]. The relative strengths and locations of upward and downward currents determine the degree to which the inner magnetosphere is penetrated by or shielded from high-latitude electric fields [*Nopper and Carovillano*, 1978]. Ionospheric conductance gradients near dusk strongly affect their intensities and directions [*Wolf*, 1970]. Quiet time sources of electric fields in the low-latitude ionosphere are thermospheric dynamos with two major contributors [*Tarpley*, 1970]. The first is UV radiation from the Sun that creates and maintains E-layer ionization. The other includes collocated thermospheric winds and tides that generate eastward electric fields in the equatorial ionosphere to drive the Sq current system. Partial closure of this current in the postdusk ionosphere gives rise to the prereversal enhancement of the eastward electric field.

[26] Severe magnetic disturbances provide another source of stormtime electric fields. During the main phase of magnetic super storms (Dst < −200 nT), electromagnetic energy (Poynting) deposition rates in the auroral oval can exceed the solar input by a wide margin [*Knipp et al.*, 2005; *Huang and Burke*, 2004]. This energy deposition creates a second thermospheric dynamo called the disturbance dynamo [*Blanc and Richmond*, 1980; *Fejer and Scherliess*, 1997; *Scherliess and Fejer*, 1997]. Computer modeling by *Blanc and Richmond* [1980] indicates that during major magnetic storms, the ionospheric disturbance dynamo driven by auroral heating produces poleward electric fields and westward plasma drifts from subauroral latitudes to the magnetic equator. *Fejer and Scherliess* [1997] noted that it takes about 10 hours of electromagnetic heating of the auroral ionosphere for the disturbance dynamos to dominate global electrodynamics. The polarity of disturbance dynamo electric fields is opposite to that of the dayside dynamo and penetration electric fields.

[27] *Heelis and Coley* [1992] accounted for local-time variations of V_Z by considering two sources of electric fields at low latitudes (<35°) during magnetic disturbance time, penetration of electric fields from the magnetosphere and the ionospheric dynamo. During quiet times, dynamo effects due to tidal motions of the neutral atmosphere at invariant latitudes <45° generally produce westward ion drift on the dayside (between 3 and 18 hours local time), and eastward ion drifts on the nightside (between 18 and 03 hours LT). They also found that increased magnetic activity adds a westward directed drift to the quiet time profile at night, at latitudes below 50°. As a result, the westward zonal drift is increased in the afternoon sector, and eastward zonal drift in the evening sector is reduced. The observed ion drift velocity during the recovery phase was indeed enhanced in the afternoon sector in agreement with this scenario. However, in the evening sector, the zonal velocity profile observed by ROCSAT-1 during the storm recovery phase indicates that eastward ion drift velocity was higher than the average drift velocity obtained by *Heelis and Coley* [1992] and *Fejer et al.* [1991], as shown in Figure 9. The observed

eastward ion drift magnitude was also greater than the typical drift velocity expected from dayside dynamo about 100 m/s [*Heelis and Coley*, 1992]. This apparent disagreement might be explained by considering additionally the shielding of PEFs in the inner magnetosphere as described earlier. The statistical drift velocity profiles deduced from radar and DE-2 measurements [*Fejer et al.*, 1991; *Heelis and Coley*, 1992] might essentially display predominantly shielding of PEFs. Eastward drift velocity becomes higher than the statistical average perhaps because of the combined effects of over shielding and disturbance dynamo at low latitudes especially during the early recovery phase of this magnetic storm.

[28] We believe that the positive azimuthal gradient in the zonal velocity observed by ROCSAT-1 at low L shells ($L < 1.5$) and the negative gradient in the equatorial azimuthal velocity detected by DMSP at the plume's L shell are connected to the penetration electric fields responsible for its formation. The large eastward ion drift observed by ROCSAT-1 in the evening hours indicates the radial electric field was inward at low L shells. Westward azimuthal SAPS flows detected by DMSP outside the plasmapause indicate large outward-directed electric fields at $L > 2.5$ in the evening sector during early recovery. This would be consistent with the interpretation that ROCSAT-1 detected effects of over-shielded magnetospheric electric fields at low L shells in the evening sector during the early recovery of this magnetic storm.

[29] Most likely the observed plasmaspheric plume formed during the storm's main phase. In the absence of EUV images during the main phase, we cannot specify how the convection profile related to the plume during the main phase. Nevertheless, simultaneous ROCSAT-1, DMSP, and IMAGE observations reported here provide new perspectives about low-latitude convection patterns near a plasmaspheric plume during the recovery phase. They demonstrate SAPS flow outside the He^+ plasmaspheric boundary on the nightside of the plume. However, DMSP F13 did not detect SAPS-like flows near the dayside edge of the plume. These observations suggest that SAPS flows were diverted radially outward at or near the plume boundary. Since cold plasma must drift along equipotential surfaces associated with the total electric field, the diversion of SAPS flow implies that the convective electric field was distorted away from typical patterns, as suggested by *Goldstein et al.* [2005]. Given the fact that SAPS manifest strong coupling between the ring current and the ionosphere, this departure from a simple pattern is not surprising.

[30] Within the plasmasphere and plume, plasma convected a little more slowly than the co-corotation velocity (Figure 6), suggesting that the dawn-to-dusk electric field was partially shielded from the plume's interior during the recovery phase. Since the SAPS was detected $\sim$1 R_E beyond the He^+ plasmaspheric boundary, SAPS-associated plasma flows follow equipotential lines outside the plasmaspheric boundary. Assuming that the plasma is incompressible, the $\nabla \bullet \mathbf{V} = 0$ condition requires that SAPS plasma should flow along the plasmaspheric boundary in the dusk sector toward the outer, dayside magnetosphere. This is the basis for a simple explanation of the observed radial diversion of SAPS flow.

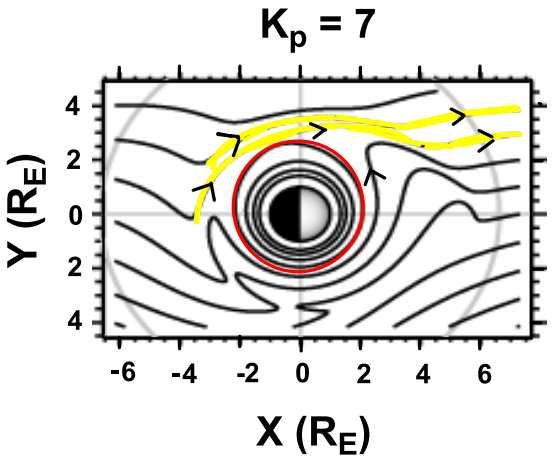

Figure 10. Equatorial magnetospheric SAPS potential model for Kp = 7. In the plot, the Earth is in the center and the Sun to the right. The potentials are produced using the SAPS potential model of *Goldstein et al.* [2005]. The red line represents the zero-energy Alfven boundary. Westward flows of SAPS plasmas are represented as yellow streamlines with black arrows.

[31] *Goldstein et al.* [2005] developed a model of SAPS potential distributions in the magnetospheric equatorial plane. They suggest that SAPS flow channels significantly alter plasma streamlines in the afternoon and evening MLT sectors. We now treat equipotentials as convection streamlines in order to compare their SAPS potential model with the flow directions observed by DMSP satellites. Figure 10 shows equipotential lines of the SAPS added to the Volland-Stern model [*Volland*, 1973; *Stern*, 1975] for Kp = 7 according to *Goldstein et al.* [2005]. We selected this activity level to represent the early recovery conditions when the Kp index decreased from 9 to 6. The red line in Figure 10 marks the zero-energy Alfvén boundary (ZEAB), the outermost closed equipotential, along which cold plasmas convect in the direction of corotation (red arrows). Outside the ZEAB, the SAPS flow is westward in the evening sector (yellow streams with black arrows). This model appears to predict more diversion of SAPS flow sunward toward the magnetopause than radially outward. The convection pattern is generally consistent with the DMSP observations during the recovery phase indicating that plasma flow pointed toward the plume MLT. However, in order to account for the pronounced plume bulge, the ZEAB's major axis should be rotated away from the dusk meridian toward afternoon.

[32] *Foster et al.* [2002] associated ionospheric Storm Enhanced Densities (SEDS) with the plasmaspheric drainage plume. Recently, *Kelley et al.* [2004] offered an explanation for density enhancements associated with SEDS. As SAPS flow moves from the dusk sector, it encounters increased conductivity on the dayside. As shown by *Wolf* [1970], equipotentials pile up near the dusk terminator with smaller poleward electric fields inside the plasmasphere than outside. As a result, zonal transport diminishes, but poleward transport continues, guiding the plume toward higher latitudes. Following their explanations, we suggest the scenario illustrated in cartoon form in Figure 11 to

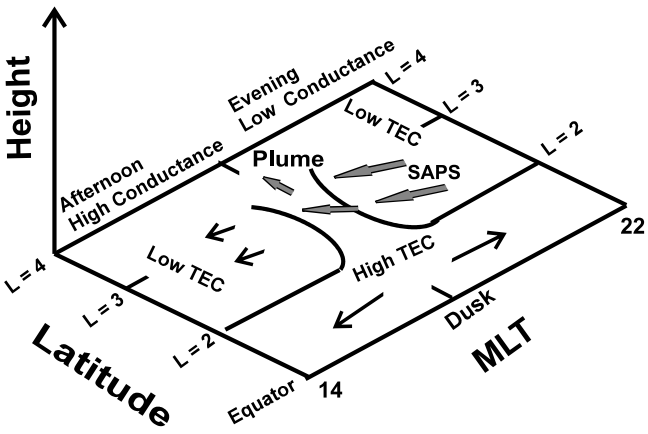

Figure 11. Scenario of plasma flow patterns in the topside ionosphere in the vicinity of the plasmaspheric drainage plume. The schematic of plasma flows is inferred from the convection patterns on the magnetospheric equatorial plane. Plasma flows are presented in Earth's corotating frame.

explain the combined ROCSAT-1 and DMSP observations. In this figure, plasma flows at the topside ionosphere are sketched in Earth's corotating frame. The plasmaspheric boundary is represented by a solid line near $L = 2$ in the afternoon and evening sectors. The boundary extends to higher latitudes near the plume. Arrows indicate initially westward SAPS flow in the evening sector. In this model, SAPS flow is diverted from westward to poleward because of the reduction of poleward electric fields inside the plasmasphere at the dusk terminator.

6. Conclusion

[33] We have reported the first observations of equatorial convection signatures associated with a plasmaspheric drainage plume using simultaneous observations from five satellites during the early recovery phase of the July 2000 Bastille Day storm. These observations provide new evidence about the diversion of SAPS flow and the distinct signatures of azimuthal velocity reversals in the vicinity of plasmaspheric plumes. Observations of three DMSP satellites indicate an azimuthal velocity reversal with a large negative gradient across the plume in the radial distance range of 2.5–3.5 R_E from Earth. ROCSAT-1 observations at low L shells, on the other hand, showed a zonal velocity reversal with a sharp positive gradient near the plume's longitude.

[34] Stormtime electric fields in the inner magnetosphere and midlatitude to low-latitude ionosphere are the main force controlling the transport and spatial distribution of cold plasma in Earth's inner magnetosphere. The stormtime electric fields in the dusk sector appear to have complicated structures inside the drainage plume and outside the plasmapause where subauroral polarization streams flow. They are superposed effects of multiple, interacting sources. The study of plasma flows in the inner magnetosphere is useful for understanding these effects and identifying contributions from various sources. Further study is needed to construct empirical models of electric fields from the observed convective velocities that would shed light on the formation of plasmaspheric boundary structures.

[35] **Acknowledgments.** We are grateful for many useful discussions with Odile de La Beaujardière. We thank the reviewers for their careful reading of the manuscript and useful suggestions. The present work was supported in part by NASA SEC-GI grant NNG04GI70G, AFOSR Task 2311AS, and Air Force contract F19628-02-C-0012 and NSF grant ATM-0334506 with Boston College. The IMAGE program at Southwest Research Institute was sponsored by NASA Contract no. NAS5-96020, and IMAGE EUV analysis was supported through a SwRI subcontract to the University of Arizona. Magnetic field mapping algorithms used in the production of Figure 5 were developed at the MIT Haystack Observatory under support of NASA Contract no. NAG5-12875 to the Massachusetts Institute of Technology. National Central University received support for this work from National Science Council of Taiwan through NSC grant 93-2111-M-008-011.

[36] Wolfgang Baumjohann thanks the reviewers for their assistance in evaluating this paper.

References

Basu, S., Su. Basu, K. M. Groves, H.-C. Yeh, S.-Y. Su, F. J. Rich, P. J. Sultan, and M. L. Keskinen (2001), Response of the equatorial ionosphere in the South Atlantic region to the great magnetic storm of July 15, 2000, *Geophys. Res. Lett.*, *28*(18), 3577–3580.

Blanc, M., and A. D. Richmond (1980), The ionospheric disturbance dynamo, *J. Geophys. Res.*, *85*(A4), 1669–1686.

Borovsky, J. E., M. F. Thomsen, D. J. McComas, T. E. Cayton, and D. J. Knipp (1998), Magnetospheric dynamics and mass flow during the November 1993 storm, *J. Geophys. Res.*, *103*(A11), 26,373–26,394.

Burke, W. J. (2006), Penetration electric fields: A Volland-Stern approach, *J. Atmos. Sol.-Terr. Phys.*, in press.

Chen, A. J., and R. A Wolf (1972), Effects on the plasmasphere of a time-varying convection electric field, *Planet. Space Sci.*, *20*, 483.

Darrouzet, F., et al. (2004), Density structures inside the plasmasphere: Cluster observations, *Ann. Geophys.*, *22*, 2577–2585.

Fejer, B. G., E. R. de Paula, S. A. Gonzalez, and R. F. Woodman (1991), Average vertical and zonal F region plasma drifts over Jicamarca, *J. Geophys. Res.*, *96*(A8), 13,901–13,906.

Fejer, B. G., and L. Scherliess (1997), Empirical models of storm time equatorial zonal electric fields, *J. Geophys. Res.*, *102*, (A11), 24047, doi:10.1029/1997JA02164.

Foster, J. C., and H. B. Vo (2002), Average characteristics and activity dependence of the subauroral polarization stream, *J. Geophys. Res.*, *107*(A12), 1475, doi:10.1029/2002JA009409.

Foster, J. C., P. J. Erickson, A. J. Coster, J. Goldstein, and F. J. Rich (2002), Ionospheric signatures of plasmaspheric tails, *Geophys. Res. Lett.*, *29*(13), 1623, doi:10.1029/2002GL015067.

Foster, J. C., A. J. Coster, P. J. Erickson, F. J. Rich, and B. R. Sandel (2004), Stormtime observations of the flux of plasmaspheric ions to the dayside cusp/magnetopause, *Geophys. Res. Lett.*, *31*, L08809, doi:10.1029/2004GL020082.

Goldstein, J., B. R. Sandel, M. R. Hairston, and P. H. Reiff (2003a), Control of plasmaspheric dynamics by both convection and sub-auroral polarization stream, *Geophys. Res. Lett.*, *30*(24), 2243 doi:10.1029/2003GL018390.

Goldstein, J., M. Spasojevic, P. H. Reiff, B. R. Sandel, W. T. Forrester, D. L. Gallager, and B. W. Reinisch (2003b), Identifying the plasmapause in IMAGE EUV data using IMAGE RPI in situ steep density gradients, *J. Geophys. Res.*, *108*(A4), 1147, doi:10.1029/2002JA009475.

Goldstein, J., B. R. Sandel, M. F. Thomsen, M. Spasojevic, and P. H. Reiff (2004), Simultaneous remote sensing and in situ observations of plasmaspheric drainage plumes, *J. Geophys. Res.*, *109*, A03202, doi:10.1029/2003JA010281.

Goldstein, J., J. L. Burch, and B. R. Sandel (2005), Magnetospheric model of substorm polarization stream, *J. Geophys. Res.*, *110*, A09222, doi:10.1029/2005JA011135.

Grebowsky, J. M. (1970), Model study of plasmaspheric motion, *J. Geophys. Res.*, *75*, 4329.

Heelis, R. A., and W. R. Coley (1992), East-west ion drifts at mid-latitudes observed by Dynamics Explorer 2, *J. Geophys. Res.*, *97*(A12), 19,461–19,469.

Huang, C. S., S. Sazykin, R. Spiro, J. Goldstein, G. Crowley, and J. M. Rouhoniemi (2006), Storm-time penetration electric fields and their effects, *EOS Trans. Amer. Geophys. U.*, *87*, 131.

Huang, C. Y., and W. J. Burke (2004), Transient sheets of field-aligned current observed by DMSP during the main phase of a magnetic storm, *J. Geophys. Res.*, 109, A06303, doi: 10.1029/2003JA010067.

Kelley, M. C., M. Vlassov, J. C. Foster, and A. J. Coster (2004), A quantitative explanation for the phenomenon known as plasmaspheric tails or storm-enhanced density, *Geophys. Res. Lett.*, *31*, L19809, doi:10.1029/2004GL020875.

Knipp, D. J., W. K. Tobiska, and B. A. Emery (2005), Direct and indirect thermospheric heating sources for solar cycles 21–23, *Sol. Phys.*, *224*, 495.

Lambour, R. L., L. A. Weiss, R. C. Elphic, and M. F. Thomsen (1997), Global modeling of the plasmasphere following storm sudden commencements, *J. Geophys. Res.*, *102*, 24,351.

Lin, C. S., H.-C. Yeh, and S.-Y. Su (2001), ROCSAT-1 satellite observations of magnetic anomaly density structures during the great magnetic storm of July 15–16, 2000, *Terr. Atmos. Ocean Sci.*, *12*, 567–582.

Lin, C.S., and H.-C. Yeh (2005), Observations of electric fields associated with magnetic anomaly density structures during the July 2000 magnetic storm,, *J. Geophys. Res.*, *110*, A03305, doi:10.1029/2003JA010215.

Mishin, E. V., W. J. Burke, C. Y. Huang, and F. J. Rich (2003), Electromagnetic wave structures within subauroral polarization streams, *J. Geophys. Res.*, *108*(A8), 1309, doi:10.1029/2002JA009793.

Moldwin, M. B., B. R. Sandel, M. Thomsen, and R. Elphic (2003), Quantifying global plasmaspheric images with in situ observations, *Space Sci. Rev.*, *109*, 47–61.

Mozer, F. S. (1970), Electric field mapping in the ionosphere at the equatorial plane, *Planet. Space Sci.*, *18*, 259–263.

Nopper, R. W., and R. L. Carovillano (1978), Polar-equatorial coupling during magnetic-ally active periods, *Geophys. Res. Lett.*, *8*, 699.

Ober, D. M., J. L. Horwitz, M. F. Thomsen, R. C. Elphic, D. J. McComas, R. D. Belian, and M. B. Moldwin (1997), Premidnight plasmaspheric "plumes", *J. Geophys. Res.*, *102*(A6), 11,325–11,334.

Sandel, B. R., R. A. King, W. T. Forrester, D. L. Gallagher, A. L. Broadfoot, and C. C. Curtis (2001), Initial results from the IMAGE Extreme Ultraviolet Imager, *Geophys. Res. Lett.*, *28*(8), 1439–1442.

Sandel, B. R., J. Goldstein, D. L. Gallagher, and M. Spasojevic (2003), Extreme ultraviolet imager observations of the structure and dynamics of the plasmasphere, *Space Sci. Rev.*, *109*, 25.

Scherliess, L., and B. J. Fejer (1997), Storm time dependence of equatorial disturbance dynamo zonal electric fields, *J. Geophys. Res.*, *102*, 24,037.

Spiro, R. W., M. Harel, R. A. Wolf, and P. H. Reiff (1981), Quantitative simulation of a magnetospheric substorm: 3, Plasmaspheric electric fields and evolution of the plasmapause, *J. Geophys. Res.*, *86*, 2261.

Stern, D. P. (1975), The motion of a proton in the equatorial magnetosphere, *J. Geophys. Res.*, *80*, 595.

Tarpley, J. D. (1970), The ionospheric wind dynamo, II Solar tides, *Planet. Space Sci.*, *18*, 1091–1103.

Thomsen, M. F., J. E. Borovsky, D. J. McCormas, R. C. Elphic, and S. Maurice (1998), The magnetospheric response to the CME passage of January 10–11, 1997, as seen at geosynchronous orbit, *Geophys. Res. Lett.*, *25*(14), 2545–2548.

Tsyganenko, N. A. (2002), A model of the near magnetosphere with a dawn-dusk asymmetry 1. Mathematical structure, *J. Geophys. Res.*, *107*(A8), 1179, doi:10.1029/2001JA000219.

Vickrey, J. F., W. E. Swartz, and D. T. Farley (1979), Ion transport in the topside ionosphere at Arecibo, *J. Geophys. Res.*, *84*(A12), 7307–7314.

Volland, H. (1973), A semiempirical model of large-scale magnetospheric electric fields, *J. Geophys. Res.*, *78*, 171.

Vasyliunas, V. M. (1970), Mathematical models of magnetospheric convection and its coupling to the ionosphere, in *Particles and Fields in the Magnetosphere*, edited by B. M. McCormac, pp. 60-71, Springer, New York.

Wolf, R. A. (1970), Effects of ionospheric conductivity on convective flow of plasma in the magnetosphere, *J. Geophys. Res.*, *75*(25), 4677–4698.

Weiss, L. A., R. L. Lambour, R. C. Elphic, and M. F. Thomsen (1997), Study of plasmaspheric evolution using geosynchronous observations and global modeling, *Geophys. Res. Lett.*, *24*, 599.

Yeh, H.-C., S. Y. Su, Y. C. Yeh, J. M. Wu, R. A. Heelis, and B. J. Holt (1999), Scientific mission of the IPEI payload on board ROCSAT-1, *TAO Supplementary Issue*, *10*, 19–42.

W. J. Burke, C. S. Lin, and F. J. Rich, Air Force Research Laboratory, Space Vehicles Directorate, Hanscom AFB, 29 Randolph Road, Bedford, MA 01731, USA. (chin.lin@hanscom.af.mil)

J. C. Foster, Haystack Observatory, MIT, Westford, MA, USA.

J. Goldstein, Southwest Research Institute, San Antonio, TX, USA.

B. R. Sandel, Lunar and Planetary Laboratory, University of Arizona, Tucson, AZ, USA.

H. C. Yeh, Institute of Space Science, National Central University, Jhongli, Taiwan.